PAPER

Check for updates

Enhancing the activity of oxygen-evolution and chlorine-evolution electrocatalysts by atomic layer deposition of TiO_2†

Cody E. Finke, [ID] ★[abc] Stefan T. Omelchenko,[c] Justin T. Jasper,[abc]
Michael F. Lichterman,[a] Carlos G. Read,[bd] Nathan S. Lewis [ID] [d] and
Michael R. Hoffmann★[abc]

We report that TiO_2 coatings formed *via* atomic layer deposition (ALD) may tune the activity of IrO_2, RuO_2, and FTO for the oxygen-evolution and chlorine-evolution reactions (OER and CER). Electrocatalysts exposed to $\sim$3–30 ALD cycles of TiO_2 exhibited overpotentials at 10 mA cm^{-2} of geometric current density that were several hundred millivolts lower than uncoated catalysts, with correspondingly higher specific activities. For example, the deposition of TiO_2 onto IrO_2 yielded a 9-fold increase in the OER-specific activity in 1.0 M H_2SO_4 (0.1 to 0.9 mA cm_{ECSA}^{-2} at 350 mV overpotential). The oxidation state of titanium and the potential of zero charge were also a function of the number of ALD cycles, indicating a correlation between oxidation state, potential of zero charge, and activity of the tuned electrocatalysts.

Broader context

Realizing a low anthropogenic CO_2 emissions future depends on the electrochemical production of fuels and commodity chemicals. In the absence of a substantial carbon tax, electrochemical production of these materials must be cost competitive with conventional production. The levelized cost of electrochemically produced chemicals depends heavily on operational expenses (OpEx; *e.g.*, buying electricity) and the balance of systems costs, and depends relatively less on the price of the catalyst.[1] Therefore, one pathway to low cost electrochemical fuel and commodity chemical production is to reduce the OpEx by fabricating highly active catalysts. Current methods to enhance catalytic activity are limited or rely on computationally-expensive calculations. Simple tools that can be used to enhance the catalytic activity for a variety of chemical reactions, such as tuning catalysts through atomic layer deposition as presented here, are essential to developing low-cost electrochemical systems that can meet global energy and chemical demands.

Introduction

Highly active electrocatalysts are required for the cost-effective generation of fuels and commodity chemicals from renewable sources of electricity.[2,3] Despite potential advantages (*e.g.*, facile product separation), the industrial use of many heterogeneous electrocatalysts is currently limited in part by suboptimal catalytic activity and/or selectivity. In addition, there are limited methods to tune the selectivity and activity of heterogeneous electrocatalysts.[2] Methods and design tools such as doping,

inducing strain, and mixing metal oxides have been used to improve the catalytic activity of heterogeneous electrocatalysts.[4–7] The activity of heterogeneous electrocatalysts can also be tuned by applying thin layers of another material, leading to an altered surface charge density on the resulting composite material relative to the bulk charge density of either individual material.[8–13] This approach has been widely used to alter the catalytic and electronic properties of core/shell nanoparticles, although additional tuning of the particle support structure is necessary to create an efficient heterogeneous electrocatalyst.[14,15] Density functional theory calculations have shown that a single atomic layer of TiO_2 on RuO_2 should lead to enhanced selectivity for the chlorine-evolution reaction (CER) relative to the oxygen-evolution reaction (OER).[9] Enhanced catalytic activity for the OER has been reported for WO_3 photocatalysts coated with 5 nm of alumina, with the activity increase ascribed to an alteration in the electronic surface-state density.[16] Enhanced catalytic activity has also been observed at the interface between TiO_2 and RuO_2, with

a The Linde Center for Global Environmental Science, Caltech, Caltech, Pasadena, CA 91125, USA
b The Resnick Sustainability Institute, Caltech, Caltech, Pasadena, CA 91125, USA
c Division of Engineering and Applied Science, Caltech, Caltech, Pasadena, CA 91125, USA. E-mail: finkec@caltech.edu, mrh@caltech.edu
d Division of Chemistry and Chemical Engineering, Caltech, Caltech, Pasadena, CA 91125, USA
† Electronic supplementary information (ESI) available. See DOI: 10.1039/c8ee02351d

358 | *Energy Environ. Sci.,* 2019, **12**, 358–365

This journal is © The Royal Society of Chemistry 2019

charge transfer between RuO_2 and TiO_2 resulting in a mixed phase with an intermediate charge density.[5]

Herein, atomic layer deposition (ALD; a stepwise deposition technique) has been used to tune the surface charge density, and consequently tune the catalytic activity, of electrocatalytic systems in a fashion consistent with estimates based on group electronegativity concepts (see Fig. S1–S5 in the ESI† for further discussion of ALD, surface homogeneity, and group electronegativity estimates). To test these predictions, the activities of the known electrocatalysts, IrO_2, RuO_2, and F-doped SnO_2 (FTO) were tuned and evaluated for the chlorine-evolution reaction (CER) and the oxygen-evolution reaction (OER). The CER provides a promising approach to infrastructure-free wastewater treatment as well as for the production of chlorine, an important industrial chemical whose global annual demand exceeds seventy million metric tons.[17,18] The OER is the limiting half-reaction for water splitting that could provide hydrogen for transportation and could also provide a precursor to energy storage *via* thermochemical reaction with CO_2 to produce an energy-dense, carbon-neutral fuel.[19]

Results and discussion

Each material tested was selected based on its theoretical group electronegativity (χ) relative to the group electronegativity of RuO_2 ($\chi \approx 2.72$), the most active catalyst for the OER in the benchmarking literature (Fig. S5, ESI†) as well as the most active catalyst for the CER.[20] IrO_2 ($\chi \approx 2.78$) and FTO ($\chi \approx 2.88$) were also investigated because they have higher electronegativities than RuO_2, and therefore using ALD to overcoat these catalysts with TiO_2 ($\chi \approx 2.62$) is expected to shift their surface electronic properties (*i.e.*, the potential of zero charge, E_{ZC}) and catalytic activities towards that of RuO_2, the optimal single metal oxide catalyst. These materials were also chosen because TiO_2, IrO_2, RuO_2, and other materials are commonly used to form mixed metal oxide electrodes, most notably the dimensionally stable anode (DSA), in which TiO_2 increases the anode's stability, but does not confer enhanced activity to the aggregated material.[21]

Overpotentials (η; the excess potential beyond the equilibrium potential required to reach a given current density) were determined for IrO_2, RuO_2, and FTO as a function of the successive number of TiO_2 ALD cycles (see ESI† for additional details on electrode preparation and testing, and TiO_2 growth rate) for the OER at 10 mA $(cm_{geo})^{-2}$ in 1.0 M H_2SO_4 and for the CER at 1 mA $(cm_{geo})^{-2}$ in 5.0 M NaCl adjusted to pH 2.0 with HCl. Current densities were chosen to produce $>95\%$ measured Faradaic efficiency for each catalyst (Table S2, ESI†), and current–potential data were corrected for the solution resistance (<2.0 mV correction) as measured by electrochemical impedance spectroscopy (see ESI† for details). The three catalysts were prepared on substrates that had very low roughness to minimize effects in geometric overpotential measurements due to surface area differences. Specifically, electrocatalyst samples consisted of a ~ 300 nm metal–oxide film sputter deposited on a (100)-oriented Si substrate, in the case of IrO_2 and RuO_2, or commercially available TEC

15 FTO glass substrates, in the case of FTO-based electrocatalysts. TiO_2 overlayers were then deposited on top of the electrocatalysts. The microstructure of a typical IrO_2-based electrocatalyst is shown in the cross-sectional scanning electron microscopy (SEM) image in Fig. 1A. The resulting electrocatalysts were very smooth with low surface roughness (Fig. 1B) such that the surface area as measured by atomic-force microscopy (AFM) was roughly equivalent to the measured geometric surface areas (Table S1, ESI†). Further characterization of the electrocatalysts' surface topology can be found in Fig. S1–S4 and Table S1 (ESI†).

Geometric overpotentials for these catalysts were considerably higher than geometric overpotentials for identical catalysts prepared on rougher substrates, however, the measured OER overpotentials at 10 mA $(cm_{geo})^{-2}$ for bare RuO_2 and IrO_2 agreed well with values reported for catalysts prepared on similarly flat surfaces. We are unaware of comparable OER data for FTO or for CER catalysts.[20,22] The overpotentials for IrO_2 and FTO, for both the OER and CER, initially showed an improvement (*i.e.*, reduction) with increasing ALD cycle number, before exhibiting an inflection point due to an increase in overpotential at higher ALD cycle numbers (Fig. 2). The triangular shape observed between the overpotential and the TiO_2 ALD cycle number is typical of a volcano-type relationship that exemplifies the Sabatier principle.[23] The overpotential reductions between bare IrO_2 and FTO catalysts and those at the peak of the volcano curve for the OER were $\Delta\eta_{OER} \approx -200$ mV at 10 cycles and -100 mV at 30 cycles, respectively. For the CER, the observed overpotential reductions were $\Delta\eta_{CER} \approx -30$ mV at 3 cycles and -100 mV at 10 cycles, for IrO_2 and FTO respectively (Fig. 2). A volcano-type relationship between cycle number and overpotential was also observed for RuO_2 facilitating the OER, with $\Delta\eta_{OER} \approx -350$ mV between 0 and 10 cycles. However, for the CER, the overpotential of the RuO_2-based catalyst increased with TiO_2 ALD cycle number (Fig. 2).

The specific activity (*i.e.*, the current density normalized to the electrochemically active surface area (ECSA)) is a standard quantity for comparing the OER activity of heterogeneous electrocatalysts (see Fig. S9–S11, and the ESI† for details on specific activity calculations and additional discussion). For IrO_2 and RuO_2 catalysts, the OER specific activities of the uncoated catalysts were in good agreement with previously reported values.[20] We are unaware of reported specific activities for FTO for the OER or for any catalyst for the CER. The specific activities for the OER and CER were characterized by volcano-type relationships as a function of the TiO_2 ALD cycle number (Fig. 2). In fact, IrO_2 coated with 10 ALD cycles of TiO_2 showed a 9-fold increase in OER specific activity at $\eta = 350$ mV relative to uncoated IrO_2. Recently, IrO_x/$SrIrO_3$ has been reported as an especially active catalyst using current normalized to atomic force microscopy measured surface area (AFMSA) in 0.5 M H_2SO_4. To compare these catalysts, we measured the roughness of our catalysts using AFM (Table S1, ESI†). For our catalysts, bare IrO_2 exhibited a Tafel slope of ~ 60 mV dec^{-1} in good agreement with previously reported OER catalysts.[24] As the activity of our IrO_2 based catalyst increased from bare IrO_2 to 10 TiO_2 ALD cycles, the Tafel slope remained constant at ~ 60 mV dec^{-1} while the

This journal is © The Royal Society of Chemistry 2019

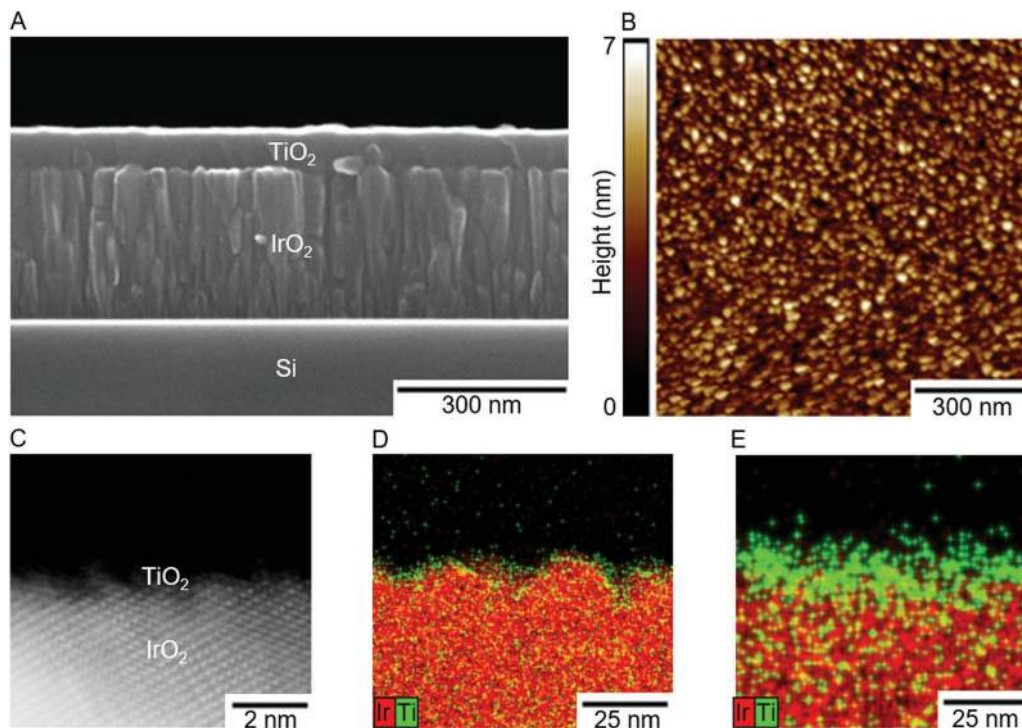*Energy Environ. Sci.*, 2019, **12**, 358–365 | 359

Fig. 1 Material characterization of typical electrocatalyst samples. (A) SEM image of an IrO_2 catalyst with 1000 ALD TiO_2 cycles. (B) AFM map of IrO_2 with 10 ALD cycles of TiO_2. (C) HAADF-STEM image of an IrO_2-based electrocatalyst with 10 ALD cycles of TiO_2. The underlying crystalline material is IrO_2 while the hair-like material at the surface is TiO_2. (D and E) Energy dispersive X-ray spectroscopy (EDS) maps of IrO_2-based electrocatalysts with 10 and 40 ALD cycles of TiO_2, respectively. The red color indicates Ir and green indicates Ti. Note that green and red intermix throughout this cross section due to the inherent roughness of the sample.

exchange current density (i_0) increased from $\sim 1 \times 10^{-7}$ to $\sim 2 \times 10^{-5}$ mA $(cm_{AFMSA})^{-2}$. Initially the $IrO_x/SrIrO_3$ catalyst also had an OER Tafel slope of ~ 60 mV dec^{-1} and an i_0 of $\sim 7 \times 10^{-6}$ mA $(cm_{AFMSA})^{-2}$. For the $IrO_x/SrIrO_3$, however, after a period of activation the Tafel slope improved dramatically to ~ 40 mV dec^{-1}, which indicates a previously unknown OER mechanism, while the i_0 deteriorated to $\sim 3 \times 10^{-7}$ mA $(cm_{AFMSA})^{-2}$ (see Fig. S11, Table S5, and ESI† for details on Tafel analysis). In our case, IrO_2 coated with 10 ALD cycles of TiO_2 exhibited lower overpotentials than the freshly prepared $IrO_x/SrIrO_3$ catalyst at current densities <1 mA $(cm_{AFMSA})^{-2}$ and lower overpotentials than the activated $IrO_x/SrIrO_3$ catalyst at <0.02 mA $(cm_{AFMSA})^{-2}$, but substantially higher overpotentials at the more industrially relevant current densities of >10 mA $(cm_{AFMSA})^{-2}$.[2,25] Further discussion on surface roughness, including AFM, and SEM sample characterization is presented in the ESI† (Fig. S1–S4 and Table S1).

To test the longevity of the enhanced catalytic performance with TiO_2 deposition, we performed 24 h stability testing at 10 mA cm^{-2} for both the CER and the OER for the uncoated catalyst and for the most active catalyst for each material system. The catalysts investigated herein were not optimized for stability and, as was previously reported for thin IrO_2 and RuO_2 catalyst depositions,[20,26] the overpotential on uncoated catalysts for the OER in 1 M H_2SO_4 degraded rapidly after <1 h of operation at 10 mA $(cm_{geo})^{-2}$. For thinly coated catalysts (3–10 cycles) the OER stability improved from about 1 h to

about 4 h, while for thicker TiO_2 coatings (>30 cycles) the OER stability increased to >9 h (Fig. S7, ESI†). The loss in activity for the OER for TiO_2 coated samples was associated with a loss in the TiO_2 coating as illustrated in X-ray photoelectron spectroscopy (XPS) measurements of the Ti 2p core level before and after electrochemical stability testing (Fig. S22, ESI†). For the CER, all catalysts were relatively stable over the 24 h testing period except for the FTO-based catalysts which followed the same trend as the OER, with thicker TiO_2 coatings stabilizing the electrodes. XPS measurements of the stable CER catalysts indicated that the TiO_2 overcoating was still present even after 24 h of continuous operation (Fig. S23, ESI†). These results indicate that, as prepared here, these catalysts are not long-term stable, and substantial work is needed to obtain an industrially relevant catalyst. Similarly prepared catalysts exhibit enhanced stability by making the catalyst material thicker, annealing the catalyst, or mixing Sb_xO_y, TiO_2, Ta_xO_y, or SnO_2 into the catalyst.[26–28] It is possible that similar techniques could be used to enhance the stability of the catalysts presented in this work.

The enhancement in catalytic performance observed with deposition of TiO_2 is not readily explained by surface morphological changes of the electrocatalyst. Deposition of TiO_2 does not substantially affect the electrochemically active surface area, a metric believed to be related to active site density, and changes in the surface area alone do not account for the magnitude of the enhancement in the specific activity (Fig. S11, ESI†).
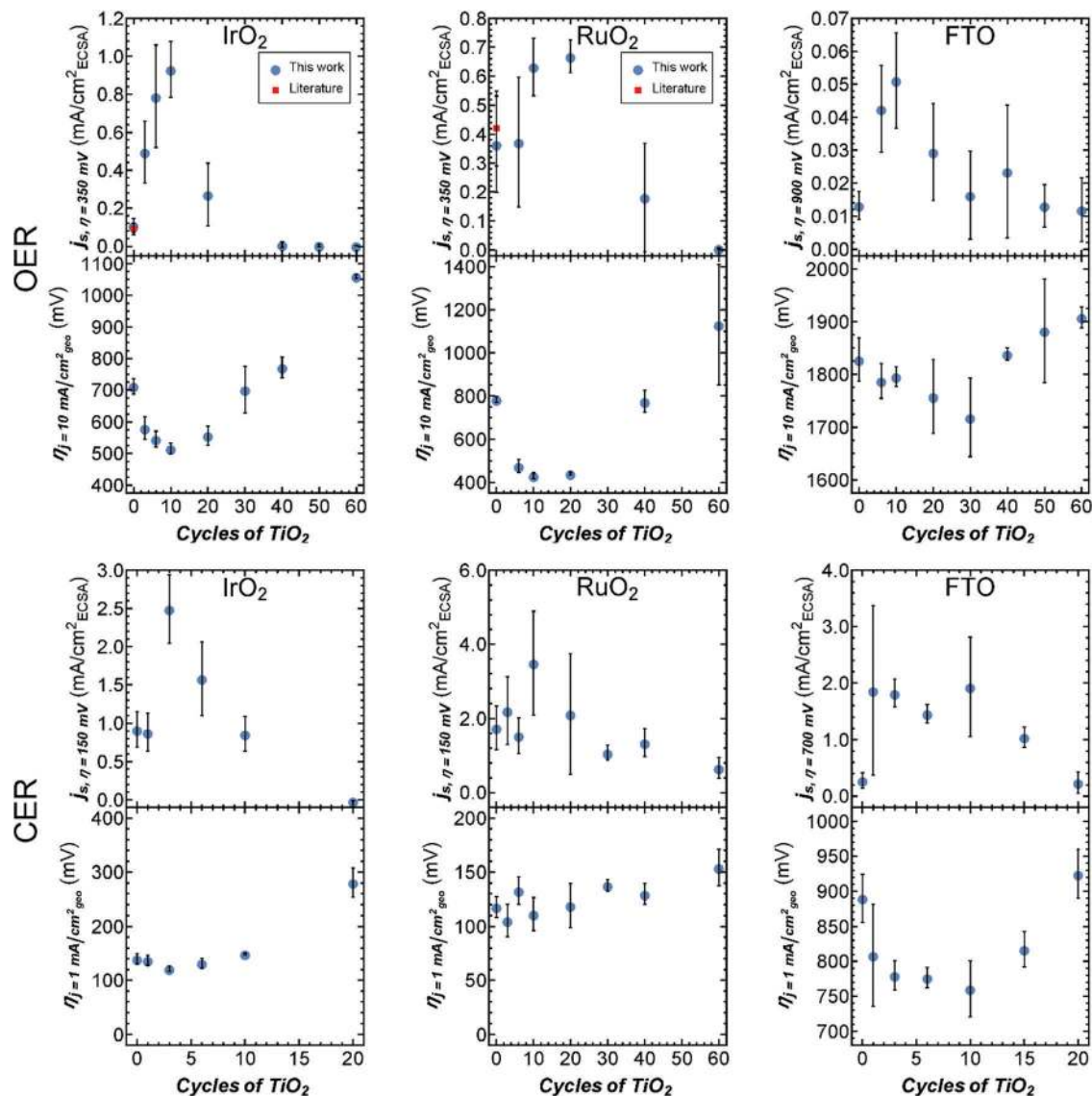
360 | Energy Environ. Sci., 2019, 12, 358–365

This journal is © The Royal Society of Chemistry 2019

Fig. 2 Specific activities (j_s) and overpotentials (η) for the OER and CER on IrO_2, RuO_2, and FTO coated at various ALD cycles of TiO_2. Overpotentials were measured at 10 mA $(cm_{geo})^{-2}$ for the OER and at 1 mA $(cm_{geo})^{-2}$ for the CER (normalized to geometric surface area). Specific activities for the OER were measured at 350 mV (IrO_2 and RuO_2) or 900 mV (FTO). Specific activities for the CER were measured at 150 mV (IrO_2 and RuO_2) or 700 mV (FTO). The red squares indicate available literature values.

Furthermore, while high-angle annular dark-field scanning transmission electron microscopy (HAADF-STEM) images and STEM electron dispersive X-ray spectroscopy (EDS) maps of IrO_2 samples with 10 cycles of TiO_2 (Fig. 1C and D) indicate that the TiO_2 film is semi-continuous with small areas of the underlying IrO_2 exposed, deposition of 40 cycles of TiO_2 results in a uniform, continuous film (Fig. 1E) and catalysis commensurate with the bare IrO_2 samples. These facts suggest the phenomenon does not arise from surface morphological effects alone, instead suggesting that TiO_2 is playing a partial role in enhancing the activity of the active sites. The idea that TiO_2 may be able to play a role in the active site is consistent with both experimental and computational literature which indicates that TiO_2 may hydrate and evolve both chlorine and oxygen.[3,29–31] The Tafel slopes for all active IrO_2 and RuO_2 based catalysts agree well with previously reported Tafel slopes

(~ 60 mV dec^{-1} and ~ 30 mV dec^{-1} for the OER and CER respectively; Tables S5, S6 and Fig. S11, ESI†),[32] consistent with expectations that addition of TiO_2 does not fundamentally change the mechanism or the potential determining step for either reaction. Hypothesized mechanisms generally involve coordination of either OOH or OCl groups to unsaturated sites on the metal oxide in the potential determining reaction steps.[33–35] FTO based catalysts exhibited very large overpotentials for both the CER and OER and had correspondingly high Tafel slopes in excess of 190 mV dec^{-1}, potentially indicating a different, much less efficient mechanism than the process that controls the reactivity of the more active catalysts.

To investigate the electrocatalysts' surface electronic properties the potentials of zero charge (E_{ZC}) of the electrocatalysts were measured as a function of TiO_2 thickness (Fig. 3). E_{ZC} is the
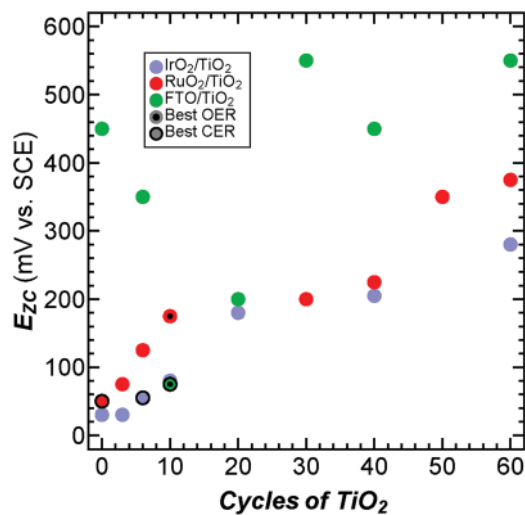
This journal is © The Royal Society of Chemistry 2019

Energy Environ. Sci., 2019, **12**, 358–365 | **361**

Fig. 3 E_{ZC} of IrO$_2$ (blue), RuO$_2$ (red), and FTO (green) anodes coated with various ALD cycles of TiO$_2$. Black dots and circles with black borders indicate the catalysts with the highest specific activity for each catalyst for the OER and CER, respectively.

potential that must be applied to produce a neutral surface and is an indicator of a material's willingness to lose electrons, with more positive E_{ZC} values indicating surfaces that are less willing to lose their electrons (see ESI,† eqn (S2) and (S3) and Fig. S12–S15 for details and discussion on handling thin TiO$_2$ layers in E_{ZC} measurements). E_{ZC} thus yields insight into the strength of the bonds on the catalyst surface.[36,37] E_{ZC} is also qualitatively very similar to group electronegativity which describes how difficult it is for molecules to gain electrons and is correlated to OER activity (Fig. S5, ESI†). Additionally, E_{ZC} of metal electrodes has been correlated with metal–oxygen single bond strengths which is also qualitatively similar to computationally derived oxygen binding energies which have long been correlated with electrocatalytic activity.[2,36,38] E_{ZC}, group electronegativity, and oxygen binding energies each have their strengths and weaknesses. E_{ZC} is measurable, but it is not easy to predict. Electronegativity is completely theoretical and very simple to calculate, but does not take into account more complex qualities of materials like edge sites. Oxygen binding energies are strongly theoretically grounded and can take into account complexities of materials like edge sites, but they are also relatively difficult to calculate. These strengths and weaknesses show that all these descriptors may be used complimentarily to predict and understand catalytic activity (Fig. S5, ESI†). Measured E_{ZC} values for bare RuO$_2$ and IrO$_2$ (50 and 30 mV vs. SCE, respectively) were consistent with previously reported values for Ru and Ir.[39] We are unaware of reported E_{ZC} values for FTO. As the RuO$_2$ and IrO$_2$ samples were coated with increasing ALD cycles of TiO$_2$ the E_{ZC} shifted from lower to higher potentials in both cases and eventually reached the value for bulk TiO$_2$. This behavior is consistent with the expected trends for equilibrated group electronegativities. The E_{ZC} for bare FTO (450 mV vs. SCE) was less than that for bulk TiO$_2$ and greater than bare IrO$_2$ or RuO$_2$. The FTO E_{ZC} decreased with increasing TiO$_2$ cycles up to 10 cycles and as the TiO$_2$ cycles increased beyond 10 the E_{ZC} increased until it reached

the bulk value of TiO$_2$ at large cycle numbers. The overall trend of the FTO E_{ZC} increasing to higher values with increasing TiO$_2$ cycle number is consistent with group electronegativity arguments. However, the intermediate behavior where the E_{ZC} decreases and then increases is not well explained by group electronegativity and could, in part, arise from the complicated behavior of the F dopant atoms (further discussion on the limits of group electronegativity are found in the ESI†). For all catalysts, the E_{ZC} continued to shift even beyond the point where TEM data indicated that the film is continuous (40 ALD cycles). This suggests that the exposed metal oxide is not fully responsible for the shift in E_{ZC} and that the surface TiO$_2$ is likely responsible in part for the E_{ZC} shift. Shifts in E_{ZC} with incremental TiO$_2$ deposition suggest that ALD can be used to tune the catalytic performance. These data reveal that the catalysts with the highest activity for the CER have E_{ZC} values between 50 and 75 mV vs. SCE (Fig. 3), consistent with the observation that addition of TiO$_2$ layers to RuO$_2$ decreased the activity of RuO$_2$ electrocatalysts (E_{ZC} = 50 mV vs. SCE) for the CER. Additionally, active OER and CER catalysts for all systems investigated have E_{ZC} values between 25 and 200 mV vs. SCE with the best OER catalysts having a somewhat higher E_{ZC} ($\sim$110 mV vs. SCE) than the best CER catalysts ($\sim$60 mV vs. SCE).

To further understand the surface states of the catalysts, X-ray photoelectron spectroscopy was used to measure the Ti oxidation state. Fig. 4 shows the Ti 2p$_{3/2}$ core-level photoemission (for the full Ti 2p region see Fig. S16, ESI†), stacked from bottom to top, for increasing ALD TiO$_2$ thickness, with 0 cycles indicating the bare catalyst substrate. Deposition of low cycle numbers of ALD TiO$_2$ on IrO$_2$ and RuO$_2$ produced Ti core-level peaks that were at $\sim$456.6 eV and $\sim$457.6 eV, which is consistent with previously reported binding energies for Ti^{3+} states.[40,41] As the ALD cycle number increased, the Ti oxidation state for these samples gradually increased to its bulk oxidation state ($\sim$+4), and signals indicative of bulk TiO$_2$ were eventually observed (Fig. 4). In the case of ALD TiO$_2$ on FTO, the lower cycle number thicknesses instead produced binding energies primarily at the bulk position, in addition to a peak at a higher binding energy. This additional peak can be ascribed to a mixed phase between the substrate (FTO) and the thin TiO$_2$ film, in which the chemical nature of the phase produces a more oxidized metal, with the mixed phase most likely dominated by Ti^{4+} sites.

The variation in the Ti oxidation state with ALD TiO$_2$ cycles was accompanied by a peak shift of the Ti 2p$_{3/2}$ peak relative to the bulk TiO$_2$ peak position (Fig. S19, ESI†). The Ti 2p$_{3/2}$ peak of the IrO$_2$- and RuO$_2$-based catalysts shifted from reduced, lower binding energies to the more oxidized, higher binding energies typical of bulk TiO$_2$. The FTO-based Ti 2p$_{3/2}$ peak shifts from more oxidized, high binding energies at low TiO$_2$ cycles to lower binding energies for intermediate TiO$_2$ cycles (10–40 cycles) before increasing again to higher binding energies at large TiO$_2$ thicknesses (>60 cycles). The Ti 2p$_{3/2}$ peak shift is qualitatively consistent with the variation in E_{ZC} with TiO$_2$ cycle number suggesting that the change in the surface charge density is correlated with a change in the Ti oxidation state.
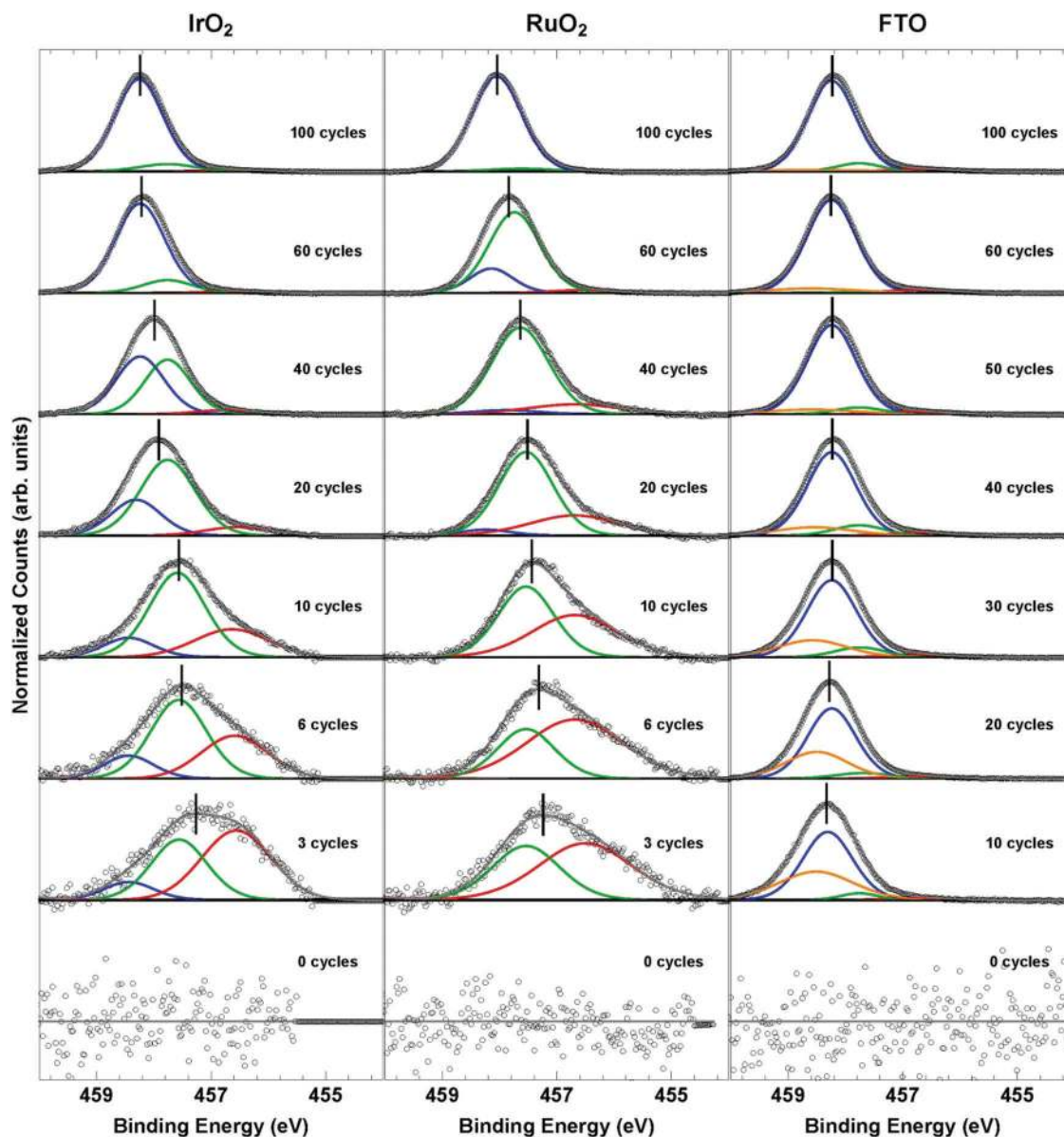
Fig. 4 X-ray photoelectron spectroscopy of the Ti 2p$_{3/2}$ region for IrO$_2$, RuO$_2$, and FTO catalysts with varying TiO$_2$ thicknesses. Bulk TiO$_2$ is shown as the blue peak in each spectrum. The slightly and highly reduced Ti peaks are shown in green and red, respectively, and the most highly oxidized Ti peak is shown in orange.

The variation in the Ti oxidation state with TiO$_2$ thickness can be explained by charge transfer from the underlying metal oxide substrate. In this scenario, a more reduced Ti species present at low deposited cycles of TiO$_2$ on IrO$_2$ and RuO$_2$ would be accompanied by a more oxidized metal oxide substrate. To confirm this hypothesis, we measured the Ir 4f, Ru 3d, and Sn 3d core-level photoemission (Fig. S20, ESI†). Unlike in the case of the Ti 2p spectra, the Ir 4f, Ru 3d, and Sn 3d core-level photoemission exhibited very small changes between the bare metal oxide substrate and those with varying thicknesses of TiO$_2$. This was reflected in the peak shifts of the main peak for the Ir 4f, Ru 3d, and Sn 3d spectra with TiO$_2$ thickness relative to that of the bare substrate (Fig. S21, ESI†), which were an order of magnitude lower than those for the Ti 2p core-level

photoemission and mostly within the error of the measurement (±0.1 eV). While peak fitting (see the ESI† for details) of these spectra indicates that initial deposition of TiO$_2$ leads to a slightly more oxidized Ir and Ru state, and a slightly more reduced Sn state for FTO, no trend with thickness was observed for any of the substrates, and changes in the oxidation state of the underlying catalyst are likely below the detection limit for the techniques used in this study (Fig. S20, S21 and Table S7, ESI†).

Conclusion

In summation, surface characterization suggests that atomic layer deposition of low cycle numbers of TiO$_2$ can tune surface

electron densities of the catalyst in a direction consistent with predictions from group electronegativity concepts (Fig. S5, ESI†). Given that concomitant changes in electrochemical activity were observed with deposition of TiO_2, these data indicate that ALD may be useful to tune the activity of other catalysts for diverse reactions, including those critical for renewable energy storage and wastewater treatment.

Conflicts of interest

The authors' institution (California Institute of Technology) has filed a U.S. patent application directly relating to the work described in the paper (patent application no. US20180087164A1, filed on Sept. 28, 2017).

Acknowledgements

Notes and references

1 M. R. Shaner, H. A. Atwater, N. S. Lewis and E. W. McFarland, *Energy Environ. Sci.*, 2016, **9**, 2354–2371.
2 Z. W. Seh, J. Kibsgaard, C. F. Dickens, I. Chorkendorff, J. K. Nørskov and T. F. Jaramillo, *Science*, 2017, **355**, eaad4998.
3 Y. Yang, J. Shin, J. T. Jasper and M. R. Hoffmann, *Environ. Sci. Technol.*, 2016, **50**, 8780–8787.
4 K. Gong, F. Du, Z. Xia, M. Durstock and L. Dai, *Science*, 2009, **323**, 760–764.
5 L.-Å. Näslund, C. M. Sánchez-Sánchez, Á. S. Ingason, J. Bäckström, E. Herrero, J. Rosen and S. Holmin, *J. Phys. Chem. C*, 2013, **117**, 6126–6135.
6 A. R. Zeradjanin, N. Menzel, W. Schuhmann and P. Strasser, *Phys. Chem. Chem. Phys.*, 2014, **16**, 13741–13747.
7 H. Li, C. Tsai, A. L. Koh, L. L. Cai, A. W. Contryman, A. H. Fragapane, J. H. Zhao, H. S. Han, H. C. Manoharan, F. Abild-Pedersen, J. K. Norskov and X. L. Zheng, *Nat. Mater.*, 2016, **15**, 48–53.
8 L. Giordano, F. Cinquini and G. Pacchioni, *Phys. Rev. B: Condens. Matter Mater. Phys.*, 2006, **73**, 045414.
9 K. S. Exner, J. Anton, T. Jacob and H. Over, *Angew. Chem., Int. Ed.*, 2014, **53**, 11032–11035.
10 R. T. Sanderson, *J. Chem. Educ.*, 1954, **31**, 2.
11 R. T. Sanderson, *Science*, 1951, **114**, 670–672.
12 R. T. Sanderson, *Chemical bonds and bond energy*, Academic Press, New York, 2nd edn, 1976.
13 R. T. Sanderson, *Chemical periodicity*, Reinhold Pub. Corp., New York, 1960.
14 Z. Zhuang, W. Sheng and Y. Yan, *Adv. Mater.*, 2014, **26**, 3950–3955.
15 L. Bu, N. Zhang, S. Guo, X. Zhang, J. Li, J. Yao, T. Wu, G. Lu, J.-Y. Ma, D. Su and X. Huang, *Science*, 2016, **354**, 1410–1414.
16 W. Kim, T. Tachikawa, D. Monllor-Satoca, H.-i. Kim, T. Majima and W. Choi, *Energy Environ. Sci.*, 2013, **6**, 3732–3739.
17 K. Cho, D. Kwon and M. R. Hoffmann, *RSC Adv.*, 2014, **4**, 4596–4608.
18 Y. P. Khalil, *Engineering*, 2015, **360**.
19 M. A. Pellow, C. J. M. Emmott, C. J. Barnhart and S. M. Benson, *Energy Environ. Sci.*, 2015, **8**, 1938–1952.
20 C. C. L. McCrory, S. Jung, I. M. Ferrer, S. M. Chatman, J. C. Peters and T. F. Jaramillo, *J. Am. Chem. Soc.*, 2015, **137**, 4347–4357.
21 S. Trasatti, *Electrochim. Acta*, 2000, **45**, 2377–2385.
22 K. A. Stoerzinger, L. Qiao, M. D. Biegalski and Y. Shao-Horn, *J. Phys. Lett.*, 2014, **5**, 1636–1641.
23 A. J. Medford, A. Vojvodic, J. S. Hummelshøj, J. Voss, F. Abild-Pedersen, F. Studt, T. Bligaard, A. Nilsson and J. K. Nørskov, *J. Catal.*, 2015, **328**, 36–42.
24 J.-M. Hu, J.-Q. Zhang and C.-N. Cao, *Int. J. Hydrogen Energy*, 2004, **29**, 791–797.
25 L. C. Seitz, C. F. Dickens, K. Nishio, Y. Hikita, J. Montoya, A. Doyle, C. Kirk, A. Vojvodic, H. Y. Hwang, J. K. Norskov and T. F. Jaramillo, *Science*, 2016, **353**, 1011–1014.
26 C. C. L. McCrory, S. Jung, J. C. Peters and T. F. Jaramillo, *J. Am. Chem. Soc.*, 2013, **135**, 16977–16987.
27 X. Chen, G. Chen and P. L. Yue, *J. Phys. Chem. B*, 2001, **105**, 4623–4628.
28 G. P. Vercesi, J. Rolewicz, C. Comninellis and J. Hinder, *Thermochim. Acta*, 1991, **176**, 31–47.
29 K. Cho and M. R. Hoffmann, *Chem. Mater.*, 2015, **27**, 2224–2233.

364 | *Energy Environ. Sci.*, 2019, **12**, 358–365

This journal is © The Royal Society of Chemistry 2019

30 M. R. Hoffmann, S. T. Martin, W. Choi and D. W. Bahnemann, *Chem. Rev.*, 1995, **95**, 69–96.

31 Y. Yang and M. R. Hoffmann, *Environ. Sci. Technol.*, 2016, **50**, 11888–11894.

32 S. Trasatti, *Electrochim. Acta*, 1984, **29**, 1503–1512.

33 M. García-Mota, A. Vojvodic, H. Metiu, I. C. Man, H.-Y. Su, J. Rossmeisl and J. K. Nørskov, *ChemCatChem*, 2011, **3**, 1607–1611.

34 H. A. Hansen, I. C. Man, F. Studt, F. Abild-Pedersen, T. Bligaard and J. Rossmeisl, *Phys. Chem. Chem. Phys.*, 2010, **12**, 283–290.

35 I. C. Man, H.-Y. Su, F. Calle-Vallejo, H. A. Hansen, J. I. Martínez, N. G. Inoglu, J. Kitchin, T. F. Jaramillo, J. K. Nørskov and J. Rossmeisl, *ChemCatChem*, 2011, **3**, 1159–1165.

36 S. Trasatti, *J. Electroanal. Chem. Interfacial Electrochem.*, 1971, **33**, 351–378.

37 S. Trasatti, *J. Electroanal. Chem. Interfacial Electrochem.*, 1972, **39**, 163–184.

38 V. Dimitrov and T. Komatsu, *J. Solid State Chem.*, 2012, **196**, 574–578.

39 A. N. Frumkin and O. A. Petrii, *Electrochim. Acta*, 1975, **20**, 347–359.

40 F. Werfel and O. Brummer, *Phys. Scr.*, 1983, **28**, 92–96.

41 D. Gonbeau, C. Guimon, G. Pfisterguillouzo, A. Levasseur, G. Meunier and R. Dormoy, *Surf. Sci.*, 1991, **254**, 81–89.

This journal is © The Royal Society of Chemistry 2019

Energy Environ. Sci., 2019, **12**, 358–365 | 365